Noise induced oscillations in a second order circuit with nonvolatile memristor

Noise induced oscillations in a second order circuit with nonvolatile memristor

Michele Bonnin
DET Department
Politecnico di Torino
Torino, Italy
michele.bonnin@polito.it

Kailing Song
DET Department
Politecnico di Torino
Torino, Italy
kailing.song@polito.it

Fernando Corinto
DET Department
Politecnico di Torino
Torino, Italy
fernando.corinto@polito.it

Fabrizio Bonani
DET Department
Politecnico di Torino
Torino, Italy
fabrizio.bonani@polito.it

Fabio L. Traversa
MemComputing Inc.
San Diego, CA, USA
ftraversa@memcpu.com

Manuel Escudero Lopez
CNR-IMM
Unit of Agrate Brianza
Agrate Brianza, Italy
manuel.escudero@mdm.imm.cnr.it

Stefano Brivio
CNR-IMM
Unit of Agrate Brianza
Agrate Brianza, Italy
stefano.brivio@mdm.imm.cnr.it

Sabina Spiga
CNR-IMM
Unit of Agrate Brianza
Agrate Brianza, Italy
sabina.spiga@mdm.imm.cnr.it

***Abstract*—The addition of a small amount of noise in nonlinears system can play an important role, inducing transitions between dynamical regimes and producing complex dynamics. In this work, we present the analysis of a second order circuit with a nonvolatile memristive device, subject to additive noise perturbations. Memristive devices are two terminal elements suitable for implementing circuits with complex dynamic behaviors, that can be used to perform bio-inspired computational tasks. We show that, depending on noise intensity, the dynamic behavior of the system undergoes multiple qualitative changes. We use numerical simulations and nonlinear dynamics concepts to analyze these transitions.**

I. Introduction

In recent years we have seen growing evidence that noise, for long considered exclusively a nuisance to be eliminated or at least reduced as much as possible, can play an important constructive role in nonlinear dynamical systems. Random noise can induce transitions between different dynamic regimes [1], and can be responsible of counter-intuitive phenomena, such as stochastic resonance [2]. A properly chosen level of noise can actually improve the performance of a system. When noise is added to a system that is initially unable to detect or transmit a weak signal, the system can exhibit enhanced sensitivity or improved signal-to-noise ratio, making the signal more detectable or easier to distinguish from background noise.

Nonlinearities can be introduced in electrical circuits through specifically designed elements. Memristive devices are two-terminal electrical elements that switch their resistance state in response of an applied stimulus. They are promising solutions for the realization of memories due to their nonvolatile properties, but they can also exhibit nonlinear and dynamic attributes, such as threshold switching, volatile switching, or negative differential resistance, that can be exploited to realize nonlinear circuits with complex dynamic behaviors [3]. For example, they can be used to design chaotic circuits [4], [5], or extremely compact oscillators exhibiting self-sustained periodic oscillations [6], [7]. Surprisingly enough, nonvolatility is rarely exploited in oscillators. For instance, a memristive device was used as a programmable resistor in conventional relaxation oscillators in [8].

In this work we propose an implementation of a simple second order nonlinear oscillator with a nonvolatile memristive device. The nonvolatile memristive device can be used as a tunable nonlinear resistor, so as to enrich the obtained dynamics. We consider here the influence of additive noise, modelled as white Gaussian noise, on the circuit dynamic response. We show how the circuit dynamics changes as the noise intensity is varied. For comparison, we also analyze the circuit dynamics when the random voltage source is replaced by a periodic source, and the interplay between noise and such periodic voltage.

II. Physical implementation of the RRAM device

In this work, we consider a resistive random-access memory (RRAM) devices consisting of 50 nm Pt/5.5 nm HfO2/40 nm TiN stacks with a 40×40 μm^2 area. Device manufacturing and modelling is described in detail in [9], [10]. After a proper electroforming procedure, the RRAM device shows resistive switching properties. Fig. 1 shows the typical $v - i$, bipolar resistive switching cycle exhibited by the device. Starting from the low resistive state (LOW), a RESET operation gradually programs the device to a high resistive state (HIGH) by applying a positive RESET voltage (in the figure, $V_{RESET} = 2$ V). Applying a properly negative voltage (V_{SET}) the opposite transition is obtained, with the device abruptly switching back to a low resistive state. LOW and HIGH are qualitative terms that refer to the RRAM device state after the SET and RESET

This work is partially supported by the PRIN2017-MIUR project COSMO (Prot. 2017LSCR4K). The research has been partially conducted within the Italian inter university PhD program in Sustainable Development and Climate Change. Correspondence to: michele.bonnin@polito.it

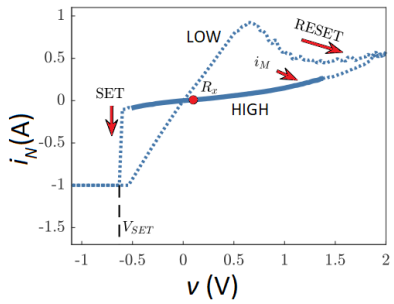

Fig. 1. Current-voltage characteristic of the realized RRAM device.

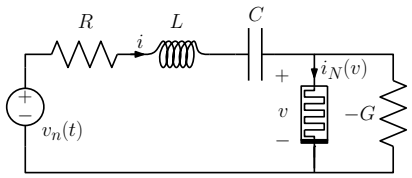

Fig. 2. Second order circuit with nonvolatile memristive device.

operations. The internal state of the device is defined through the resistance $R(x)$ at 0.1 V, as shown in Fig. 1.

The $v-i$ characteristics in the HIGH resistive state is strongly nonlinear. A polynomial fitting of the measurements shows that the $v-i$ characteristics can be modelled as a fifth order polynomial

$$i_N(v) = \sum_{k=1}^{5} G_k\, v^k \tag{1}$$

where the conductance coefficients are summarized in table I.

III. Circuit Model and Results

We have used the RRAM device to implement a programmable nonlinear resistor in a second order nonlinear oscillator, shown in Fig. 2. The circuit is composed of two reactive elements, an inductor and a capacitor, connected in series with a linear resistor. A random voltage source is included, to model external and internal noise, such as thermal noise in the linear resistor or the influence of the environment. A shunted resistor, characterized by negative conductance $(-G)$ is connected in parallel with the nonvolatile memristive element, that provides the nonlinearity thanks to its nonlinear $v-i$ characteristic.

Using Kirchhoff laws, the following state equations are derived:

$$\frac{dx_1}{d\tau} = x_2 - R\, i_N(x_1) + R\, G\, x_1 \tag{2a}$$

$$\frac{dx_2}{d\tau} = -\frac{R^2 C}{L}(x_1 + x_2) + \frac{R^2 C}{L}\, v_n(\tau) \tag{2b}$$

where $x_1 = v$, $x_2 = R\, i$ are the normalized voltages, $i_N(x_1)$ is the $v-i$ characteristic assumed for the memristor and $\tau = t/(RC)$ is the dimensionless time . Circuit's parameters used in our analysis are summarized in table I.

R = 49.820 kΩ	L = 24.82 H	C = 10 nF
$G_1 = 1.91$ μS	$G_2 = 0.31$ μS/V	$G_3 = 19.1$ μS/V^2
$G_4 = -5.2$ μS/V^3	$G_5 = 1.77$ μS/V^4	$G = 33.893$ μS

TABLE I
Circuit's parameters

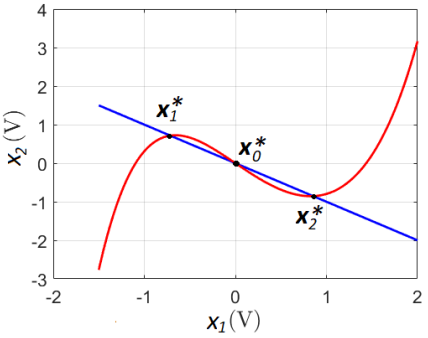

Fig. 3. Nullclines showing locations of equilibrium points

The autonomous system is obtained setting $v_n(\tau) = 0$. It exhibits three equilibrium points, that can be located by looking at the intersections of the nullclines (the set of points such that $dx_1/d\tau = dx_2/d\tau = 0$), as shown in Fig. 3. By looking at the eigenvalues of the Jacobian matrix

$$J(x_1, x_2) = \begin{bmatrix} RG + R\, i_N'(x_1) & 1 \\ -R^2C/L & -R^2C/L \end{bmatrix} \tag{3}$$

it turns out that the origin $\mathbf{x}_0^*$ is an unstable equilibrium of saddle type (two real valued eigenvalues, one positive and one negative), whereas $\mathbf{x}_1^*$ and $\mathbf{x}_2^*$ are asymptotically stable equilibrium points of focus type (complex conjugate eigenvalues with negative real parts). The basins of attraction of the two stable equilibrium points are separated by the separatrix, represented by the stable manifold $W^s_{\mathbf{x}_0^*}$ of the saddle point, the red line shown in Fig. 4.

IV. Noise Analysis

To investigate the influence of noise, we have assumed that the voltage source is a white Gaussian process, and we have

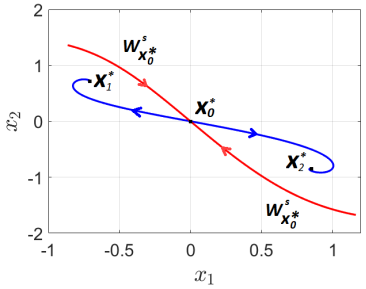

Fig. 4. Equilibrium points and their stable/unstable manifolds for the autonomous circuits. Blue lines are the unstable manifolds of the saddle equilibrium point. $W^s_{\mathbf{x}_0^*}$ (the red line) is the stable manifold, which is also the separatrix between the basins of attraction of stable equilibria.

integrated the resulting stochastic differential equations using two different stochastic integration methods: Euler-Maruyama and stochastic Runge-Kutta method with strong order of convergence equal to one. Under this assumption, equation (2) becomes a system of stochastic differential equations (SDE system):

$$d\mathbf{X}_t = \mathbf{n}(\mathbf{X}_t)dt + \mathbf{B}\, dW_t \tag{4}$$

where $\mathbf{X}_t : \Omega \times [0, +\infty] \mapsto \mathbb{R}^2$ is a vector of stochastic processes (Ω is a sample space) that defines the state of the circuit, $\mathbf{n} : \mathbb{R}^2 \mapsto \mathbb{R}^2$ is a smooth vector field that satisfy a Lipschitz condition to guarantee existence and uniqueness of the solutions, and $\mathbf{B}$ is a constant vector. Finally W_t is a Wiener process, also called Brownian motion, the integral of a white Gaussian noise.

Because matrix $\mathbf{B}$ is constant, noise is unmodulated, or additive. In this case the two main interpretations adopted for SDEs, namely Itô or Stratonovich, coincide. In our analysis, to perform computations we have adopted the Itô interpretation. It is worth mentioning that, for SDE systems, the change of variables and change of time formula is different from the ordinary differential equations case. In particular, for a linear change of variables $\mathbf{Y} = \mathbf{P}\mathbf{X}$, where $\mathbf{P}$ is a regular matrix, and the change of time $\tau = \omega t$, $\omega > 0$, if $\mathbf{X}_t$ is a solution of (4), then $\mathbf{Y}\tau$ solves:

$$d\mathbf{Y}_\tau = \frac{1}{\omega}\,\mathbf{P}\,\mathbf{n}(\mathbf{P}^{-1}\mathbf{Y}_\tau)d\tau + \frac{1}{\sqrt{\omega}}\,\mathbf{P}\mathbf{B}\, dW_\tau \tag{5}$$

Moreover, $\mathbf{X}_t$ and $\mathbf{Y}_\tau$ converge only weakly, i.e. they coincide only in distribution [11], [12]. As a consequence, only information about the probability distribution can be inferred from the scaled SDEs.

Application of equation (5), transforms the SDE system (2) into:

$$dx_1 = (x_2 - R\, i_N(x_1) + R\,G\,x_1)d\tau \tag{6a}$$

$$dx_2 = -\frac{R^2C}{L}(x_1 + x_2)d\tau + D\frac{R}{L}\sqrt{RC}\, dW_\tau \tag{6b}$$

where D denotes the noise strength.

The SDE system (6) has been solved numerically, using both the two methods mentioned above. The time simulation length was set to $\Delta\tau = 10^4$ (dimensionless time), the number of samples was $N = 2^{27}$, and the fixed time integration step was $\delta\tau = \Delta\tau/N \approx 7.45 \cdot 10^{-5}$.

For small values of the noise intensity the voltages exhibit small random fluctuations around one of the two stable equilibrium points, which one ultimately determined by the initial condition, as it can be seen in Fig. 5(a). Fig. 5(b) shows the corresponding marginal probability density function (PDF) $p(x_1, \tau)$, for τ large enough. The PDF shows a single peak, centred around one of the stable equilibrium points. It is worth mentioning that for $\tau \to +\infty$, the system is expected to shows transitions from the basin of attraction of one equilibrium point to the other with probability one. This is because the variance of the Wiener process grows unbounded with time. However, on a finite time scale and for small enough noise intensities, no transition is observed.

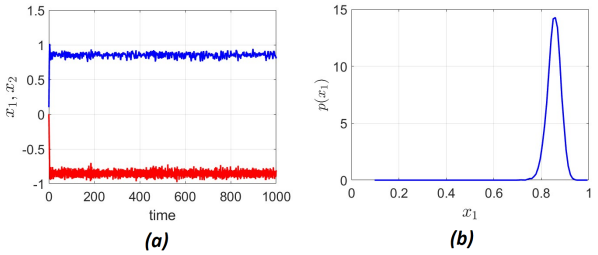

Fig. 5. **(a)** Normalized voltages x_1 (blue line) and x_2 (red line) versus time. **(b)** Marginal probability density function $p(x_1)$. Normalized noise intensity is $D = 10^{-3}$.

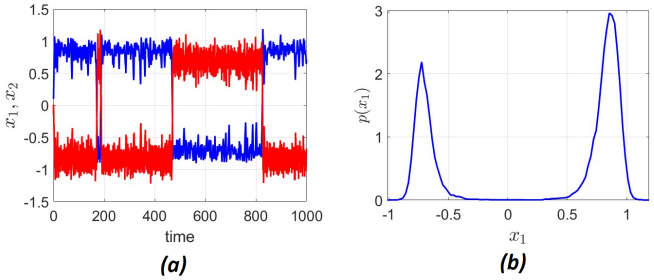

Fig. 6. **(a)** Normalized voltages x_1 (blue line) and x_2 (red line) versus time. **(b)** Marginal probability density function $p(x_1)$. Normalized noise intensity is $D = 3 \cdot 10^{-3}$.

If the noise intensity is increased, amplitude of fluctuations increases correspondingly. When the noise intensity exceeds a certain threshold, random jumps occur between the basins of attraction of the two equilibrium points, and the circuit dynamics resemble that of a particle in a double-well potential. The corresponding PDF for large, but still finite τ, shows two peaks centred at the two equilibrium points, see Fig. 6.

Finally, if the noise intensity is further increased, the state variables exhibits approximately regular jumps between the two basins of attraction, resembling random relaxation oscillations (Fig. 7). The marginal PDF still shows two marked peaks, but the peaks begin to merge together, as it can be seen from the fact that the PDF is not null at $x_1 = 0$. At this point, the amplitude of fluctuations shows little to no dependence at all on the noise intensity. Any variation of the latter, only reflects into a change of the switching frequency between the two basins of attraction.

It is worth noticing that although the dynamic behaviour of the circuit resembles that of a particle in a two wells potential, the SDE system (6) is not a system with a quartic potential. Instead, bi-stability is a consequence of the nonlinear resistance. To understand the mechanism originating the random relaxation oscillations, we introduce the coordinates transformation

$$x = x_1 \tag{7a}$$

$$y = x_2 - R\, i_N(x_1) + R\,G\,x_1 \tag{7b}$$

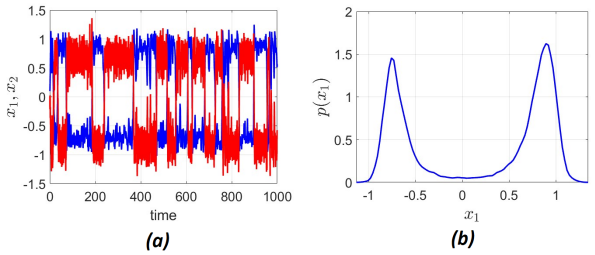

Fig. 7. **(a)** Normalized voltages x_1 (blue line) and x_2 (red line) versus time. **(b)** Marginal probability density function $p(x_1)$. Normalized noise intensity is $D = 5 \cdot 10^{-3}$.

Using Itô formula, the SDE system (6) transforms into

$$dx = y\, d\tau \tag{8a}$$

$$dy = (-U'(x) - F(x)\, y)d\tau + D\frac{R}{L}\sqrt{RC}\, dW_\tau \tag{8b}$$

where $U'(x) = x + R\, i_N(x) - RG\, x$ and $F(x) = -RG + R\, i'_N(x) + 1$. The SDE system (8) describes a nonlinear oscillator with potential $U(x)$, subject to the nonlinear dissipation $F(x)\, y$. In the absence of noise, the differential equation (8) admits three equilibrium points at $U'(x) = 0$, $y = 0$. Equilibrium points corresponding to the minima of $U(x)$ are asymptotically stable, whereas the origin, which corresponds to a local maximum of $U(x)$, is unstable of saddle type. In the presence of noise, the state of the system fluctuates within one of the two potential wells of $U(x)$, with random oscillations corresponding to jumps between the two potential wells. Transitions from one potential well to the other occur when the trajectory crosses the separatrix between the basins of attraction of the equilibrium points. In particular, when the trajectory reaches the separatrix, there is a 50% probability of transition into the other potential well. Interestingly, transitions do not occur near the saddle point. Fig. 8 shows an example of transition. The trajectory of the noisy circuit is shown by the black line, the stable manifold of the saddle $W^s_{\mathbf{x}^*_0}$ is in red, while the unstable manifold of the saddle $W^u_{\mathbf{x}^*_0}$, which coincides with the stable manifold of the other equilibrium points $W^s_{\mathbf{x}^*_{1,2}}$ is in blue. Starting from a random initial condition, the noisy trajectory is attracted by the stable equilibrium point. it converges to it following its stable manifold $W^s_{\mathbf{x}^*_2}$. The trajectory does not necessarily reach $\mathbf{x}^*_2$, but it fluctuates around the equilibrium. If during its random wandering, the state comes close enough to $W^s_{\mathbf{x}^*_0}$, it is attracted by the saddle and starts to follow the separatrix. However the manifold $W^s_{\mathbf{x}^*_0}$ is stable only along one direction. Any perturbation transversal to the manifold is amplified, and the trajectory may be either pushed back towards $\mathbf{x}^*_2$, or it may cross the separatrix and converge towards the other equilibrium point $\mathbf{x}^*_1$, again following the manifold $W^u_{\mathbf{x}^*_0} \equiv W^s_{\mathbf{x}^*_1}$. Because the probability distribution has peaks centred at $\mathbf{x}^*_1$ and $\mathbf{x}^*_2$, and shows a minimum at $\mathbf{x}^*_0$, we expect that the separatrix crossing occurs where the distance between $W^u_{\mathbf{x}^*_0}$ and the equilibrium points is minimum.

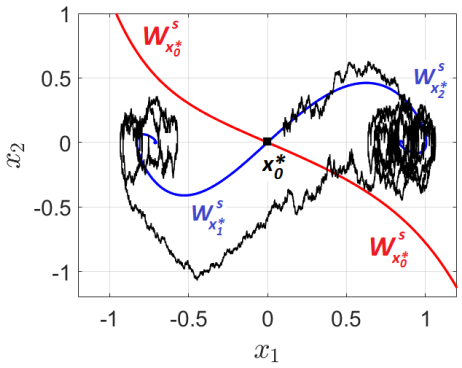

Fig. 8. Example of trajectory of the noisy circuit (black line), compared to invariant manifolds of the deterministic system (blue and red lines).

V. Conclusions

We report on the effect of small additive noise in a second order circuit with a nonvolatile memristive device. The memristive device makes the circuit, and the governing equations, nonlinear. We show that increasing the noise intensity, the circuit exhibits transition from small amplitude random fluctuations, to large amplitude random oscillations. An explanation of this transition is given, based on an analogy with bifurcations induced by a simple periodic forcing.

References

[1] W. Horsthemke, "Noise induced transitions," in *Non-Equilibrium Dynamics in Chemical Systems: Proceedings of the International Symposium, Bordeaux, France, September 3–7, 1984*. Springer, 1984, pp. 150–160.

[2] L. Gammaitoni, P. Hänggi, P. Jung, and F. Marchesoni, "Stochastic resonance," *Reviews of modern physics*, vol. 70, no. 1, p. 223, 1998.

[3] S. Kumar, X. Wang, J. P. Strachan, Y. Yang, and W. D. Lu, "Dynamical memristors for higher-complexity neuromorphic computing," *Nature Reviews Materials*, vol. 7, no. 7, pp. 575–591, 2022.

[4] B. Muthuswamy, "Implementing memristor based chaotic circuits," *International Journal of Bifurcation and Chaos*, vol. 20, no. 05, pp. 1335–1350, 2010.

[5] S. Sabarathinam, C. K. Volos, and K. Thamilmaran, "Implementation and study of the nonlinear dynamics of a memristor-based duffing oscillator," *Nonlinear Dynamics*, vol. 87, pp. 37–49, 2017.

[6] N. Shukla, A. Parihar, E. Freeman, H. Paik, G. Stone, V. Narayanan, H. Wen, Z. Cai, V. Gopalan, R. Engel-Herbert *et al.*, "Synchronized charge oscillations in correlated electron systems," *Scientific reports*, vol. 4, no. 1, p. 4964, 2014.

[7] S. Kumar, J. P. Strachan, and R. S. Williams, "Chaotic dynamics in nanoscale nbo2 mott memristors for analogue computing," *Nature*, vol. 548, no. 7667, pp. 318–321, 2017.

[8] Y. V. Pershin and M. Di Ventra, "Practical approach to programmable analog circuits with memristors," *IEEE Transactions on Circuits and Systems I: Regular Papers*, vol. 57, no. 8, pp. 1857–1864, 2010.

[9] S. Brivio, J. Frascaroli, and S. Spiga, "Role of metal-oxide interfaces in the multiple resistance switching regimes of pt/hfo2/tin devices," *Applied Physics Letters*, vol. 107, no. 2, 2015.

[10] J. Frascaroli, F. G. Volpe, S. Brivio, and S. Spiga, "Effect of al doping on the retention behavior of hfo2 resistive switching memories," *Microelectronic Engineering*, vol. 147, pp. 104–107, 2015.

[11] K. Song, M. Bonnin, F. L. Traversa, and F. Bonani, "Moment-based stochastic analysis of a bistable energy harvester with matching network," *Applied Sciences*, vol. 13, no. 6, p. 3880, mar 2023.

[12] ——, "Stochastic analysis of a bistable piezoelectric energy harvester with a matched electrical load," *Nonlinear Dynamics*, vol. 111, no. 18, pp. 16 991–17 005, 2023.